

## Disrupted structural and functional brain networks in Alzheimer's disease



Zhengjia Dai<sup>a,b,1</sup>, Qixiang Lin<sup>a,c,1</sup>, Tao Li<sup>d,e,f</sup>, Xiao Wang<sup>d,e,f</sup>, Huishu Yuan<sup>g</sup>, Xin Yu<sup>d,e,f</sup>, Yong He<sup>a,c,\*\*</sup>, Huali Wang<sup>d,e,f,\*</sup>

<sup>a</sup> National Key Laboratory of Cognitive Neuroscience and Learning & IDG/McGovern Institute for Brain Research, Beijing Normal University, Beijing, China

<sup>b</sup> Department of Psychology, Sun Yat-sen University, Guangzhou, China

<sup>c</sup> Beijing Key Laboratory of Brain Imaging and Connectomics, Beijing Normal University, Beijing, China

<sup>d</sup> Dementia Care & Research Center, Peking University Institute of Mental Health (Sixth Hospital), Beijing, China

<sup>e</sup> Beijing Key Laboratory for Translational Research on Diagnosis and Treatment of Dementia, Beijing, China

<sup>f</sup> National Clinical Research Center for Mental Disorders (Peking University Sixth Hospital), Beijing, China

<sup>g</sup> Department of Radiology, Peking University Third Hospital, Beijing, China

### ARTICLE INFO

#### Article history:

Received 29 January 2018

Received in revised form 8 November 2018

Accepted 9 November 2018

Available online 16 November 2018

#### Keywords:

Structural connectivity  
Functional connectivity  
Small-world  
Connectome  
Graph theory

### ABSTRACT

Studies have demonstrated that the clinical manifestations of Alzheimer's disease (AD) are associated with abnormal connections in either functional connectivity networks (FCNs) or structural connectivity networks (SCNs). However, the FCN and SCN of AD have usually been examined separately, and the results were inconsistent. In this multimodal study, we collected resting-state functional magnetic resonance imaging and diffusion magnetic resonance imaging data from 46 patients with AD and 39 matched healthy controls (HCs). Graph-theory analysis was used to investigate the topological organization of the FCN and SCN simultaneously. Compared with HCs, both the FCN and SCN of patients with AD showed disrupted network integration (i.e., increased characteristic path length) and segregation (i.e., decreased intramodular connections in the default mode network). Moreover, the FCN, but not the SCN, exhibited a reduced clustering coefficient and reduced rich club connections in AD. The coupling (i.e., correlation) of the FCN and SCN in AD was increased in connections of the default mode network and the rich club. These findings demonstrated overlapping and distinct network disruptions in the FCN and SCN and a strengthened correlation between FCNs and SCNs in AD, which provides a novel perspective for understanding the pathophysiological mechanisms underlying AD.

© 2018 Elsevier Inc. All rights reserved.

### 1. Introduction

Understanding the neural mechanisms of Alzheimer's disease (AD) is crucial, as AD is a progressive neurodegenerative disease characterized by a decline in memory processing and cognitive function. Neuroimaging research has demonstrated that the clinical manifestations of patients with AD are associated not only with structural and functional damage in specific brain regions but also

with decreased connections between different brain regions (defined as the disconnection mechanisms of AD) (Delbeuck et al., 2003, 2007). With the advent of noninvasive structural and functional neuroimaging techniques, researchers have been able to capture AD-related disconnection patterns using graph theoretical analysis (i.e., the connectome) (Dai and He, 2014; He et al., 2009a; Sporns et al., 2005). A better understanding of the connectome-based disruptions in AD may help bridge the gap between pathological processes and emerging clinical manifestations. It also allows uncovering why the disease propagates along specific paths.

In the past decade, connectome-based methods revealed many nontrivial topological organizations of healthy human brain networks: a high clustering coefficient and modular structure, which reflects network segregation in the human brain, and low characteristic path length, significant rich club structure (dense interconnections among a small set of highly connected brain regions), and high nodal degree centrality, which reflects network integration in the human brain (Bullmore and Sporns, 2009; He and

\* Corresponding author at: Dementia Care & Research Center, Peking University Institute of Mental Health (Sixth Hospital), Beijing, China. Tel.: +86-10-82801983; fax: +86-10-62011769.

\*\* Corresponding author at: National Key Laboratory of Cognitive Neuroscience and Learning, IDG/McGovern Institute for Brain Research, Beijing Key Laboratory of Brain Imaging and Connectomics, Beijing Normal University, Beijing, China. Tel.: +86-10-58802036; fax: +86-10-58802036.

E-mail addresses: [yong.he@bnu.edu.cn](mailto:yong.he@bnu.edu.cn) (Y. He), [huali\\_wang@bjmu.edu.cn](mailto:huali_wang@bjmu.edu.cn) (H. Wang).

<sup>1</sup> These authors contributed equally to this work.

Evans, 2010; Liao et al., 2017; van den Heuvel and Sporns, 2011). Related to AD, numerous previous studies have reported changes in topological properties of either functional connectivity networks (FCNs) or structural connectivity networks (SCNs). Using resting-state functional magnetic resonance imaging (R-fMRI), several FCN studies revealed decreased network segregation (e.g., decreased clustering coefficient and modular structure) (Chen et al., 2013; Supekar et al., 2008) and increased network integration (e.g., decreased characteristic path length) (Sanz-Arigita et al., 2010) in patients with AD compared with healthy controls (HCs). In contrast, using diffusion MRI (dMRI), several SCN studies discovered increased network segregation (e.g., increased clustering coefficient) (Daianu et al., 2013) and decreased network integration (e.g., increased characteristic path length) (Lo et al., 2010) in AD. Regarding the rich club structures and hubs in the network in AD, studies also showed considerable variability across studies (for review, see Tijms et al., 2013). Despite the fact that these studies revealed abnormal network segregation and integration of the FCN and SCN in AD, these findings were inconsistent between studies of FCNs and SCNs. One possibility could be that previous studies recruited different AD populations or examined different MRI modalities. For example, the SCN represents anatomical wiring diagrams, whereas the FCN reflects the synchronization of neuronal activities in different brain regions. Hence, it is crucial to investigate the topological properties of FCNs and SCNs in the same cohort of AD. However, very few studies have been performed in this manner.

In addition to investigating the independent role of the FCN and SCN in AD, studies also need to consider the relationship between the FCN and SCN. Recently, researchers have argued that the FCN of the brain could be constrained by the underlying SCN (Hagmann et al., 2010; Honey et al., 2009, 2010; Park and Friston, 2013; Wang et al., 2015c). A growing body of research has focused on the relationship between SCNs and FCNs from the perspectives of connectivity (Hermundstad et al., 2013; Honey et al., 2009; Skudlarski et al., 2008), subnetworks (Greicius et al., 2009; van den Heuvel et al., 2009), and network topology (Alexander-Bloch et al., 2013; Park et al., 2008). Intriguingly, the coupling (i.e., correlation coefficient) of FCNs and SCNs has been found to be significantly correlated with brain development (Hagmann et al., 2010) and change in brain diseases, including stronger FCN-SCN coupling in schizophrenia (van den Heuvel et al., 2013) and decreased FCN-SCN coupling in idiopathic generalized epilepsy (Zhang et al., 2011). Studying the changes in the FCN-SCN coupling may provide a potential biomarker that detects subtle brain connectivity disruption more sensitively than does a single modality (van den Heuvel et al., 2013; Zhang et al., 2011; for review, see Wang et al., 2015b) and facilitate a mechanistic understanding of the dynamic change in clinical manifestations. However, it remains largely unknown whether the FCN-SCN coupling is changed in patients with AD.

To address the aforementioned issues, in the present study, we collected R-fMRI and dMRI data from the same cohort of patients with AD and matched HCs, followed by graph theoretical analyses to systematically examine the topological properties of the FCN, SCN, and the FCN-SCN coupling. We sought to determine (1) whether the patients with AD from the same cohort show overlapping and distinct disruptions in the topological organization in the FCN and SCN and (2) whether the FCN-SCN coupling of brain networks changes in AD at different levels, including the whole brain, subnetworks, and nodal degree levels. We hypothesized that the FCN and SCN would show common topological measure alterations in the AD. In addition, considering that different MRI modalities provide different types of information, we hypothesized that the FCN and SCN would show distinct topological measure alterations in patients with AD, and the FCN-SCN coupling would also be disrupted in the AD. As described previously, previous

studies using different MRI modalities (e.g., R-fMRI and dMRI) and different samples showed a lack of consistent direction regarding the between-group differences in network properties. Thus, we tested this hypothesis without specifying the expected direction for group comparisons.

## 2. Materials and methods

### 2.1. Participants

Patients with AD and HCs were recruited to establish a registry at the Dementia Care and Research Center, Peking University Institute of Mental Health. After enrollment, each participant underwent a comprehensive clinical interview, a neuropsychological battery assessment, laboratory tests, and multimodal brain MRI examinations. Participants in the registry were also invited to receive follow-up tests every 6 months. For this study, we selected patients (registered between June 2007 and May 2011) who had a baseline diagnosis of AD and had completed an MRI examination before initiation of nootropic medication ( $n = 47$ ). All participants were right-handed Han Chinese. All participants were clinically assessed with the Clinical Dementia Rating (CDR) (Morris, 1993), which categorized them as HCs ( $CDR = 0$ ) or as patients in the early stage of AD ( $CDR \geq 0.5$ ). The clinical diagnosis of AD was made according to the International Classification of Disease, 10th Revision (ICD-10) (World Health Organization, 1999) and the criteria for probable AD of the National Institute of Neurological and Communicative Disorders and the Stroke/Alzheimer's Disease and Related Disorders Association (NINCDS-ADRDA) (McKhann et al., 1984). Patients were excluded if they presented structural abnormalities that could result in dementia, such as cortical infarction, tumor, or subdural hematoma, or if they had concurrent illnesses other than dementia that interfered with cognitive functions at the time of the MRI examination. The HCs had no history of neurological or psychiatric disorders, sensorimotor impairment, or cognitive complaints; no abnormal anatomical findings by conventional brain MRI; and no evidence of cognitive deficits from neuropsychological tests. Written informed consent was obtained from each participant, and this study was approved by the institutional review board of the Peking University Institute of Mental Health. A subset of this data set was used to examine the APOE- $\epsilon 4$ -mediated modulation of large-scale brain networks, hippocampal structure, and function, and cognitive performance (Wang et al., 2015a,b). In the present study, 87 participants (47 AD patients and 40 HCs) were selected. The data of 1 patient with AD and 1 HC were discarded because of excessive motion artifacts during the R-fMRI scan (see [Image preprocessing](#)). The clinical and demographic data of the remaining 85 participants are summarized in [Table 1](#).

### 2.2. Neuropsychological assessment

All participants performed a Chinese version of the Mini-Mental State Examination (MMSE) and the cross-cultural neuropsychological test battery (Dick et al., 2002), including the Cognitive Abilities Screening Instrument (CASI) (Teng et al., 1994), the Common Objects Memory Test (COMT) (Kempler et al., 2010), the Consortium to Establish a Registry for Alzheimer's Disease (CERAD) verbal category fluency, auditory comprehension, picture completion, digit span (forward and backward), and Trail-Making Test A. Among these neuropsychological measures, the MMSE and CASI are comprehensive cognitive screeners that cover a wide range of cognitive functions. The MMSE is a standardized cognitive state examination tool and screener of AD, and the CASI tests abilities associated with memory, attention, orientation, language, visual construction, abstraction, and judgment. To obtain more robust

**Table 1**  
Demographic, clinical and cognitive characteristics of the participants

Variables	AD (n = 46)	HCS (n = 39)	p-value
Age (years)	73.37 ± 5.67	71.03 ± 6.79	0.086
Sex (M/F)	16/30	16/23	0.554
Education (years)	13.74 ± 3.23	13.41 ± 3.80	0.667
CDR	0.5 (n = 22), 1 (n = 24)	0	-
MMSE	21.39 ± 3.43	28.62 ± 1.53	<0.001 <sup>c</sup>
CASI	78.35 ± 9.22	95.41 ± 3.42	<0.001 <sup>c</sup>
Episodic memory <sup>a</sup>	-0.63 ± 0.64	0.72 ± 0.27	<0.001 <sup>c</sup>
COMT Trial 1 <sup>a</sup>	4.24 ± 1.49	6.79 ± 1.28	<0.001 <sup>c</sup>
COMT Trial 2 <sup>a</sup>	5.56 ± 1.91	8.36 ± 1.25	<0.001 <sup>c</sup>
COMT Trial 3 <sup>a</sup>	5.84 ± 1.85	8.94 ± 1.04	<0.001 <sup>c</sup>
Free delayed recall—5-min	3.28 ± 2.54	8.79 ± 1.34	<0.001 <sup>c</sup>
Recognition—5-min	17.67 ± 2.23	19.97 ± 0.16	<0.001 <sup>c</sup>
Free delayed recall—30-min	2.65 ± 2.67	8.69 ± 1.03	<0.001 <sup>c</sup>
Recognition—30-min <sup>a</sup>	17.89 ± 2.54	19.97 ± 0.16	<0.001 <sup>c</sup>
Executive function <sup>b</sup>	-0.24 ± 0.38	0.29 ± 0.36	<0.001 <sup>c</sup>
Verbal fluency	11.70 ± 3.50	19.59 ± 3.51	<0.001 <sup>c</sup>
Auditory comprehension <sup>a</sup>	23.36 ± 1.96	24.62 ± 0.67	<0.001 <sup>c</sup>
Picture completion <sup>b</sup>	5.89 ± 2.22	7.74 ± 2.10	<0.001 <sup>c</sup>
Digit span <sup>a</sup>	13.62 ± 4.03	16.46 ± 3.81	0.001 <sup>c</sup>
Digit span—forward <sup>a</sup>	8.31 ± 2.33	10.08 ± 2.31	<0.001 <sup>c</sup>
Digit span—backward <sup>a</sup>	5.53 ± 2.83	6.33 ± 2.41	0.171
Trail-Making Test A—time (seconds) <sup>a</sup>	118.33 ± 67.60	53.26 ± 15.23	<0.001 <sup>c</sup>

Data were presented as the mean (SD); *p*-values were obtained using the two-tailed Chi-square test for sex and two-tailed two-sample *t*-tests for other variables.

Key: AD, Alzheimer's disease; HCs, healthy controls; CDR, Clinical Dementia Rating; MMSE, Mini-Mental State Examination; CASI, Cognitive Ability Screening Instrument; COMT, Common Object Memory Test.

<sup>a</sup> Data were missing for 1 patient.

<sup>b</sup> Data were missing for 1 patient and 1 HC.

<sup>c</sup> *P* < 0.05, Bonferroni corrected.

measures and increase statistical power, we used a composite score analysis of these neuropsychological measures. Briefly, for each participant, the raw scores of each neuropsychological measure were first transformed to Z scores by subtracting the mean test scores and being divided by the standard deviation of the test scores across all participants (85 participants). Then, the composite scores were calculated by averaging the Z scores for episodic memory (7 tests, including COMT Trial 1, COMT Trial 2, COMT Trial 3, 5-min free delayed recall, 5-min recognition, 30-min free delayed recall, and 30-min recognition) and executive function (5 tests, including verbal fluency, auditory comprehension, picture completion, digit span, and the Trail-Making Test A).

### 2.3. MRI data acquisition

All participants were scanned on a 3-Tesla MR system (Siemens Magnetom Trio, A Tim system, Germany) using a standard 8-channel head coil. Foam pads and headphones were used to minimize participants' head motion and scanner noise. A three-dimensional, T1-weighted magnetization-prepared rapidly acquired gradient-echo (MPRAGE) sequence was used to acquire high-resolution anatomical images using the following parameters: repetition time (TR)/echo time (TE) = 2530 ms/3.44 ms; time inversion (TI) = 1100 ms; slice number = 192; slice thickness = 1.0 mm; gap = 0 mm; matrix = 256 × 256; and field of view (FOV) = 256 × 256 mm<sup>2</sup>. The scan time of this sequence was approximately 360 seconds. The R-fMRI data were collected using an echo-planar imaging (EPI) sequence: interleaved axial slices, TR/TE = 2000 ms/30 ms; flip angle = 90°; slice number = 30; slice thickness = 4.0 mm; gap = 0.8 mm; matrix = 64 × 64; and FOV = 220 × 220 mm<sup>2</sup>. Before the scan, the participants were instructed to keep their eyes closed but not to fall asleep, relax their mind, and move as little as possible during data acquisition. The R-fMRI scan lasted for 420 seconds in total. A simple questionnaire confirmed that no participant had fallen asleep during the R-fMRI scan. The dMRI sequence was acquired using a spin-echo single-shot EPI sequence: TR/TE = 5300 ms/92 ms; 64 nonlinear diffusion

directions with *b* = 1000 s/mm<sup>2</sup> and an additional volume with *b* = 0 s/mm<sup>2</sup>; repetition = 2; voxel size = 1.8 × 1.8 × 3.3 mm; slice thickness = 3.0 mm; gap between slices = 0.3 mm; matrix = 128 × 128; and FOV = 230 × 230 mm<sup>2</sup>. The scan lasted 706 seconds.

### 2.4. Image preprocessing

#### 2.4.1. R-fMRI data

Unless stated otherwise, all R-fMRI data were preprocessed using Statistical Parametric Mapping (SPM8, <http://www.fil.ion.ucl.ac.uk/spm>) and Data Processing Assistant for Resting-State fMRI (DPARSF) (Yan and Zang, 2010). Briefly, the first 5 functional volumes were discarded to allow for stabilization of the initial signal and adaptation of the participants to the circumstances. The remaining fMRI images were then corrected for acquisition time delay between slices and further realigned to the first volume to correct for head motion. The data of 2 participants (1 AD with CDR = 0.5 and 1 HC) were excluded based on a head motion criterion of 3 mm translation and 3° rotation. Next, the individual T1-weighted image was coregistered to the mean functional image after motion correction using a linear transformation (Collignon et al., 1995) and was then segmented into gray matter (GM), white matter, and cerebrospinal fluid tissue probabilistic maps using a unified segmentation algorithm with SPM's priori tissue maps as reference (Ashburner and Friston, 2005). The motion-corrected functional volumes were spatially normalized to the Montreal Neurological Institute (MNI) space using the normalization parameters estimated during unified segmentation. The spatially normalized functional images were resampled to 3-mm isotropic voxels and underwent linear detrending. Then, the nuisance signals (Friston's 24 head motion parameters and 5 CompCor signals; Behzadi et al., 2007) were regressed out from the time course of each voxel. The Friston's 24 head motion parameters (i.e., 6 head motion parameters, 6 head motion parameters 1 time point before, and 12 corresponding squared items) (Friston et al., 1996) were used here as recent studies suggest that higher-order

models minimize the effects of head motion (Satterthwaite et al., 2013; Yan et al., 2013). Finally, the residual signals were temporally bandpass filtered (0.01 Hz–0.1 Hz) to reduce the effect of low-frequency drifts and high-frequency physiological noise (Biswal et al., 1995; Lowe et al., 1998).

#### 2.4.2. Diffusion MRI data

Unless stated otherwise, all dMRI data were preprocessed using FMRIB's Diffusion Toolbox (FSL, version 5.0, [www.fmrib.ox.ac.uk/fsl](http://www.fmrib.ox.ac.uk/fsl)). First, an affine transformation was used to align the diffusion-weighted images to the b0 image to correct the eddy current distortions and the motion artifacts in the dMRI data set. Next, the diffusion tensor of each voxel was estimated by solving the Stejskal and Tanner equation, and the reconstructed tensor matrix was diagonalized to obtain 3 eigenvalues ( $\lambda_1, \lambda_2, \lambda_3$ ) and the corresponding eigenvectors. The fractional anisotropy (FA) of each voxel was then calculated using the 3 eigenvalues.

### 2.5. Network construction

In this study, functional and structural brain networks were constructed at the macroscale with nodes representing brain regions, which were obtained by parcellating the brain GM (excluding the cerebellum) into 625 similar-sized regions that preserved automated anatomical labeling (AAL) landmarks (Crossley et al., 2013; Tzourio-Mazoyer et al., 2002; Zalesky et al., 2010). Fourteen regions were excluded because the number of voxels with nonzero standard deviations of blood oxygen level-dependent (BOLD) time series in that region was less than half of the total number of voxels in that region in some participants. Finally, 611 regions of interest (ROIs, AAL-611) were used to define the network nodes. Data processing steps are shown in Fig. 1.

#### 2.5.1. Construction of FCNs

To acquire the functional connectivity for each participant, Pearson's correlation coefficients and the significance levels between the time series of each pair of ROIs were calculated. Considering the ambiguous biological explanation of negative correlation (Fox et al., 2009; Murphy et al., 2009), we restricted our analysis to positive correlation connections and set the negative correlation coefficients as zero. Therefore, for each participant, we obtained a  $611 \times 611$  symmetric positive functional connectivity (FC) matrix with the Fisher-transformed version of Pearson's correlation coefficients as weight. To further assess the topological properties of

FCNs, we generated a binary and undirected  $611 \times 611$  network for each participant through a thresholding procedure. The correlation coefficients with  $p$ -values less than a statistical threshold ( $p < 0.05$ , Bonferroni corrected) were set as 1 or 0 otherwise.

#### 2.5.2. Construction of SCNs

The procedure for brain structural network construction was similar to our previous studies (Gong et al., 2009; Shu et al., 2011). In brief, individual T1-weighted images were coregistered to the b0 image in native diffusion space using a linear transformation. The transformed T1-weighted images were then spatially normalized to the ICBM152 T1 template in the MNI space, and the transformation matrix was inverted to warp AAL-611 atlases from the MNI space to the native diffusion space with a nearest-neighbor interpolation method to keep the label values as integral numbers. Reconstruction of the whole-brain white matter tracts was performed using DtiStudio software (version 3.0.3) based on the Fiber Assignment by the Continuous Tracking (FACT) algorithm (Mori et al., 1999). All tracts in the data set were computed by seeding each voxel with an FA greater than 0.2. The fiber-tracking was terminated if it turned an angle greater than  $45^\circ$  or reached a voxel with an FA less than 0.2. As a result, all the fiber pathways within the brain were reconstructed using a deterministic tractography method. For each edge, we calculated the connection density (Honey et al., 2009) as follows:

$$w_{ij} = \frac{2}{S_i + S_j} \sum_{f \in E_{ij}} 1/l(f),$$

where  $S_i$  and  $S_j$  were the cortical surfaces of node  $i$  and node  $j$ ,  $l(f)$  was the length of fiber  $f$  along its trajectory, and  $E_{ij}$  was the set of all fiber streamlines connecting node  $i$  and node  $j$ . Therefore, for each participant, we obtained a  $611 \times 611$  symmetric structural connectivity (SC) matrix with the connection density as weighted. To further assess the topological properties of SCNs, we generated a binary and undirected  $611 \times 611$  network for each participant with the structural connectivity between 2 regions set as 1 if the corresponding weight was positive.

### 2.6. Network analysis

We systematically analyzed both the global and regional properties of the FCN (binary and undirected  $611 \times 611$  network) and the SCN (binary and undirected  $611 \times 611$  network), including

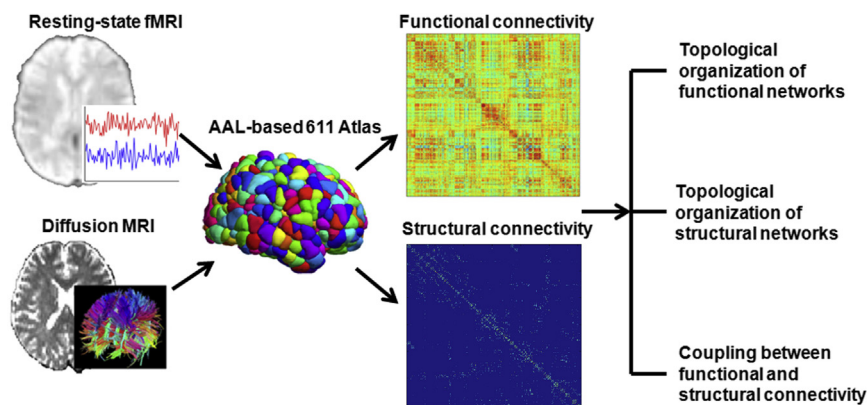


**Fig. 1.** A brief flowchart of constructing FCNs and SCNs and exploring the relationship between FCNs and SCNs. First, based on the AAL-611 template, we parcellated the brain gray matter into 611 distinct brain regions. Then, for preprocessed resting-state fMRI data, Pearson's correlation coefficients between the time series of each pair of regions were calculated to obtain the  $611 \times 611$  FCN. For preprocessed diffusion MRI data, the deterministic tractography method was used to obtain the  $611 \times 611$  SCN. Finally, the topological organization of FCNs and SCNs and the coupling of the FCN and SCN were examined between patients with AD and HCs. For more details, see [Materials and Methods](#). Abbreviations: FCN, functional connectivity network; SCN, structural connectivity network; AAL, automated anatomical labeling; AD, Alzheimer's disease; HCs, healthy controls.

whole-brain network attributes (i.e., clustering coefficient  $C_p$ , characteristic path length  $L_p$ , normalized clustering coefficient  $\gamma$ , normalized characteristic path length  $\lambda$ , and small-worldness  $\sigma$ ), subnetwork attributes (i.e., modularity and rich club organization), and the nodal property (i.e., degree). High clustering coefficient  $C_p$ , normalized clustering coefficient  $\gamma$ , and modularity reflect the network segregation in the brain, which is the ability for specialized neuronal processing carried out among densely interconnected regions. The low characteristic path length  $L_p$ , the normalized characteristic path length  $\lambda$ , the significant rich club organization, and high nodal degree centrality show the network integration in the brain, which is the ability for global information communication or distributed network integration. The small-worldness  $\sigma$  characterizes an optimized balance between network segregation and integration. To identify brain functional modules, the FCN was subjected to a modularity analysis. Specifically, given that the module number and membership vary between participants, we performed the modularity analysis on the group level. The group functional network was generated by selecting all connections that were present in at least 70% of the HCs. Then, a spectral optimization algorithm was used to detect the modular structure based on the group functional network of the HCs (Newman, 2006). Furthermore, to explore the reliability of the modular structure (Cohen and D'Esposito, 2016; Geib et al., 2017), the algorithm was repeated 1000 times. Then, we measured the similarity between the first partition and the other partitions with the normalized mutual information (Lancichinetti et al., 2008). We found the range of normalized mutual information from 0.975 to 1, indicating very similar module assignments across different partitions. Given the highly comparable module partitions, we used the first partition result as the final module assignment. Based on the modular structure, the intramodular connectivity was calculated as the sum of the connections within a module, whereas the intermodule connectivity was calculated as the sum of the connections between any pair of 2 modules. The modules used in the SCN were based on the modules of the group functional network of HCs. In addition, we also extracted the modular structure based on the group functional network of AD and found that the between-group differences of the modular measures (i.e., intramodular and intermodule functional connections) were consistent with those based on the partition of group functional network of HCs. The rich-club phenomenon is that a small number of highly connected nodes constitute a densely interconnected “rich club.” The rich club plays a central role in information communication (Colizza et al., 2006) and has been found in human brain structural networks (van den Heuvel and Sporns, 2011). For a binary structural network of each participant, the rich club nodes were defined as the nodes with a degree (i.e., the number of edges connected to the node) larger than  $k$ . Based on the rich club nodes of the SCN, the rich club connections of the FCN and SCN were calculated as the number of the edges among the rich club nodes. Here, we chose a range of  $k$  values from 11 to 17 (i.e., corresponding to approximately 20%–5% of the network nodes). To determine the nodal characteristics of the FCN and SCN, we computed the nodal degree (i.e., the number of edges connected to the node: a node with a larger degree allows more efficient communications across brain regions). This measure showed high test-retest reliability in the brain functional networks (Liao et al., 2013; Wang et al., 2011). It was tightly correlated with the brain's physiological measures such as regional cerebral blood flow, oxidative glucose metabolism, and aerobic glycolysis (Liang et al., 2013; Tomasi et al., 2013; Vaishnavi et al., 2010). For more detailed descriptions and interpretations of these network measures, see Rubinov and Sporns (2010) and Supplemental Information.

## 2.7. Coupling between functional and structural connectivities

We explored the relationship between FC and SC matrices and networks at the following 5 levels. (1) Whole-brain connectivity level—For each participant, the coupling between FC and SC matrices was examined by computing the correlation between the functional connectivity (i.e., Fisher-transformed version of Pearson's correlation coefficients) and structural connectivity (density), which was constrained by the edges with nonzero structural connections. Specifically, the nonzero structural connections were first extracted to produce a structural connectivity vector. Then, we resampled these values into a gaussian distribution with a mean of 0.5 and a standard deviation of 0.1 (Honey et al., 2009). The corresponding functional connectivities were also extracted as a vector. Finally, Pearson's correlation between the 2 vectors was calculated to quantify the coupling between the FC and SC. (2) Small-worldness level—For each network measure (i.e.,  $C_p$ ,  $L_p$ ,  $\gamma$ ,  $\lambda$ , and  $\sigma$ ) and each group, a cross-participant Pearson's correlation analysis between the network measure of the FCN and that of the SCN was performed to examine the coupling of small-worldness between functional and structural networks. (3) Modularity level—For each participant, once the functional module structure was defined, a correlation analysis was performed on the connections within modular/intermodule between the FC and SC matrices. Specifically, for each module, the nonzero structural connectivities within the module were first extracted to produce a structural connectivity vector. Then, we resampled these values, extracted the corresponding functional connectivities (i.e., Fisher-transformed version of Pearson's correlation coefficients) as a vector and calculated the Pearson's correlation, using the same method as used for the whole-brain connectivity level to obtain the coupling values at the modularity level. (4) Rich club level—For each participant, based on rich club nodes, we calculated the correlations within the rich club between FC (i.e., Fisher-transformed version of Pearson's correlation coefficients) and SC matrices, using the same method as used for the whole-brain connectivity level. (5) Nodal level—For each participant and each node, the coupling degree was calculated as the number of common edges of functional and structural connectivities with the given node. Specifically, we can obtain the functional connectivity vector and structural connectivity vector of the given node, respectively. The number of common edges of the 2 vectors was defined as the coupling degree.

## 2.8. Statistical analysis

To examine between-group differences in network properties, a general linear model analysis was performed with age, gender, and education level as covariates. Notably, for each nodal measure analysis, a false discovery rate (FDR) procedure was further performed at a  $p$  value of 0.05 to correct for multiple comparisons (i.e., 611 regions). Finally, the relationship between network properties with significant between-group differences and cognitive measures (i.e., MMSE, CASI, episodic memory, and executive function) was calculated in the AD and HC groups, respectively, after controlling for age, gender, and education level. The FDR procedure was also performed at a  $p$  value of 0.05 to correct for multiple comparisons (i.e., multiple network properties and the 4 cognitive measures).

## 2.9. Validation analysis

We evaluated whether our main results were influenced by 2 other alternative head motion correction strategies and connectivity density thresholds. (1) Different head motion correction strategies: Recent studies have suggested that head motion has a confounding effect on functional connectivity analysis (Power et al., 2012;

Satterthwaite et al., 2013; Van Dijk et al., 2012; Yan et al., 2013). In this study, to minimize the effects of head motion, we have used CompCor methods and Friston's 24 head motion parameters regression methods to correct the motion artifacts (Muschli et al., 2014; Satterthwaite et al., 2013; Yan et al., 2013). In addition, we found nonsignificant differences in head motion between AD and HC groups (two-tailed two-sample *t*-test,  $p = 0.131$ , for the mean framewise displacement [FD] of Jenkinson; Jenkinson et al., 2002). Nonetheless, to validate our main results, 2 alternative head motion correction strategies were performed: (1) We reanalyzed functional data by including mean FD as an additional covariate (Chen et al., 2018; Yan et al., 2013) in group analysis. (2) We performed a scrubbing procedure on the preprocessed images (Power et al., 2012; Yan et al., 2013). For each participant, we deleted the volumes with FD > 0.5 mm together with 1 previous volume and the 2 following volumes, and the network metrics were then reanalyzed using these censored R-fMRI data. (2) Connectivity density thresholds: In this study, we used a statistically significant correlation method to threshold the connections. This method enables the examination of the absolute topological organization of functional networks. In addition, we also analyzed the network metrics using a fixed-density threshold (10%, 15%, and 20%, the minimum network density across the participants based on the statistically significant correlation method is 9.1%) as a complementary analysis, ensuring the same number of connections across all participants.

### 3. Results

#### 3.1. Demographic data and cognitive performance

There were no significant differences in age, gender, and education level between AD and HC groups (all  $p > 0.05$ , Table 1). As expected, the patients with AD had significantly lower performance than HCs in all the cognitive domains (i.e., MMSE, CASI, episodic memory, and executive function). Demographic data and cognitive performance of the 85 participants are shown in Table 1.

#### 3.2. Disrupted functional connectivity network

Compared with HCs, patients with AD had significantly lower functional connection strength ( $p = 0.034$ ) and fewer number of edges ( $p = 0.029$ ) in the FCN. For topology organization, compared with HCs, patients with AD exhibited a significantly decreased clustering coefficient ( $p = 0.023$ ) and increased characteristic path length

( $p = 0.010$ ), normalized clustering coefficient ( $p = 0.022$ ), and normalized characteristic path length ( $p = 0.005$ ), and small-worldness ( $p = 0.027$ ). Based on the group functional network of HCs, we visually identified 5 modules (modularity value = 0.470) based on previous atlas/studies (He et al., 2009b; Liang et al., 2015; Power et al., 2011; Yeo et al., 2011): default mode network (DMN), executive-control network (ECN), salience network (SN), somatosensory-motor network (SMN), and visual network (VN) (Fig. 2A). The intramodular functional connection numbers of the DMN, SN, and ECN were significantly decreased (all  $p < 0.05$ , Fig. 2B) in patients with AD compared with HCs. Decreased intermodule connectivity was located among the SN, SMN, and VN (all  $p < 0.05$ , Fig. 2B) in the AD group compared with HCs. For the rich club analysis, the functional connection numbers were significantly reduced in AD for rich club connections when  $k$  varies from 11 to 13 (all  $p < 0.05$ , Table 2). At the nodal level, compared with HCs, the AD showed a decreased nodal degree in the left hippocampus and inferior fusiform gyrus, right amygdala, superior temporal pole, middle temporal pole, and inferior temporal gyrus ( $p < 0.05$ , FDR corrected, Fig. 2C).

#### 3.3. Disrupted structural connectivity network

Compared with the HCs, patients with AD had a lower structural connection density ( $p = 0.035$ ) and a fewer number of edges ( $p = 0.033$ ) of the SCN. For topology organization, the AD group showed only increased characteristic path length ( $p = 0.019$ ) with no change in other small-worldness measures (all  $p > 0.05$ ). Based on the modular organization of the group functional network of HCs, we found that the DMN exhibited decreased intramodular structural connectivity. The number of structural connectivities between ECN and other 4 modules (i.e., DMN, SMN, VN, and SN) was significantly decreased in patients with AD compared with HCs (all  $p < 0.05$ , Fig. 3A). For the rich club analysis, no significant difference in rich club connections was found (all  $p > 0.05$ ). At the nodal level, compared with HCs, the AD group showed a decreased nodal degree in the right middle frontal gyrus, insula, and middle temporal gyrus ( $p < 0.05$ , FDR corrected, Fig. 3B).

#### 3.4. Disrupted functional connectivity and structural connectivity network coupling

At the whole-brain connectivity level, both the AD and HC groups showed significant correlations between the whole SC and FC (all  $p < 10^{-37}$ ), but there was no significant difference in these

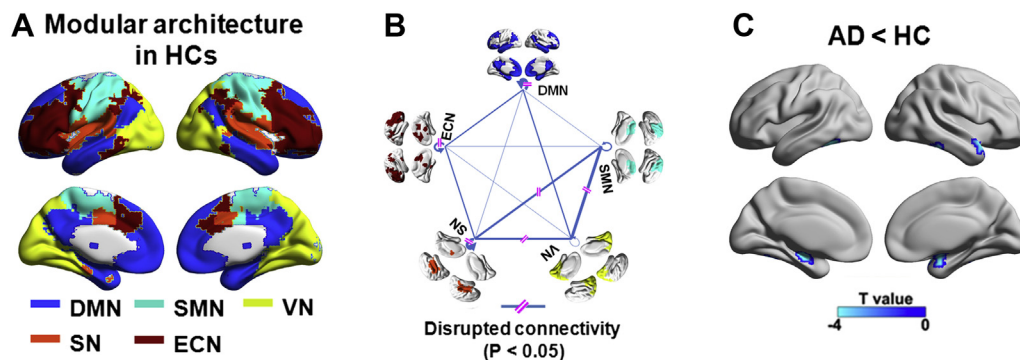


**Fig. 2.** Alterations of modular structure and nodal degree of FCNs in patients with AD relative to HCs. (A) Five modules were identified for the group-level mean network of HCs, including DMN, SMN, VN, SN, and ECN. (B) AD-related intramodular and intermodule functional connectivities decrease ( $p < 0.05$ ). The intramodular connectivity was calculated as the sum of the connection within a module, whereas the intermodule connectivity was calculated as the sum of the connection between any pair of 2 modules. The line width represents the *t*-value of between-group comparison (all AD < HCs). (C) Between-group difference of nodal degree of FCNs ( $p < 0.05$ , FDR corrected). The results were mapped on the brain surface using BrainNet Viewer (Xia et al., 2013). Abbreviations: FCN, functional connectivity network; DMN, default mode network; SMN, somatosensory-motor network; VN, visual network; SN, salience network; ECN, executive-control network; AD, Alzheimer's disease; HCs, healthy controls.

**Table 2**  
Summary of network topology difference between the patients with AD and HCs

Index	FCN	SCN	FC-SC coupling
$C_p$	-2.323 (0.023)	NS	NS
$L_p$	2.631 (0.010)	2.405 (0.019)	NS
$\gamma$	2.333 (0.022)	NS	NS
$\lambda$	2.872 (0.005)	NS	NS
$\sigma$	2.257 (0.027)	NS	NS
Connections within DMN	-3.546 (0.0007) <sup>a</sup>	-2.039 (0.045)	2.026 (0.046)
Connections within SMN	NS	NS	NS
Connections within VN	NS	NS	NS
Connections within SN	-3.717 (0.0004) <sup>a</sup>	NS	NS
Connections within ECN	-2.353 (0.021)	NS	NS
DMN-SMN connections	NS	NS	NS
DMN-VN connections	NS	NS	NS
DMN-SN connections	NS	NS	NS
DMN-ECN connections	NS	-2.808 (0.006)	NS
SMN-VN connections	-2.679 (0.009)	NS	NS
SMN-SN connections	-2.509 (0.014)	NS	NS
SMN-ECN connections	NS	-2.026 (0.046)	NS
VN-SN connections	-2.515 (0.014)	NS	NS
VN-ECN connections	NS	-2.104 (0.039)	NS
SN-ECN connections	NS	-2.459 (0.016)	NS
Rich club (k = 11)	-2.483 (0.015)	NS	NS
Rich club (k = 12)	-2.289 (0.025)	NS	NS
Rich club (k = 13)	-2.163 (0.034)	NS	NS
Rich club (k = 17)	NS	NS	2.134 (0.036)

Data are presented as t-score (*p*-value).

Key: NS, nonsignificant; AD, Alzheimer's disease; HCs, healthy controls; DMN, default mode network; SMN, somatosensory-motor network; VN, visual network; SN, salience network; ECN, executive-control network; FC, functional connectivity; SC, structural connectivity.

<sup>a</sup> *p* < 0.05, FDR corrected.

correlation coefficients between the 2 groups (*p* = 0.363). At the small-worldness level, there were no significant correlations of the topological measures across participants in each group (all *p* > 0.05) and no significant difference of the 2 Fisher's r-to-z transformed correlation coefficients between groups (all *p* > 0.05). At the modularity level, significantly stronger FC-SC correlations were found in the DMN module (*p* = 0.046, Fig. 4A) in the AD group compared with HCs. At the rich club level, significantly increased FC-SC correlations were found in the rich club connections of the

AD group compared with HC group when *k* equaled 17 (*p* = 0.036, Fig. 4B). At the nodal level, we found that a significantly decreased coupling degree located in the right rectus and insula, and the bilateral medial prefrontal gyrus, inferior frontal gyrus, middle temporal gyrus, and hippocampus. (*p* < 0.05, FDR corrected; Fig. 4C).

### 3.5. Relationships between network metrics and cognitive performance

After the FDR correction, no significant correlations between network metrics and cognitive performance were found in the AD or HC group.

### 3.6. Validation results

We assessed the effects of head motion correction and connectivity density thresholds on our main findings. (1) The effect of head motion: Using both the statistical analysis accounting for mean FD as a covariate in the between-group comparisons and the scrubbing procedure, we found that the main results were not affected (Table S1 in Supplemental Information). Moreover, decreased intermodule functional connectivity was also found in AD among the SN, ECN, and DMN after controlling for FD in the statistical model. Using the scrubbing procedure, we found decreased intermodule functional connectivity in AD between the SN and ECN, DMN. Note that in the scrubbing analysis, to guarantee stable results, the participants with time points of R-fMRI data less than 5 minutes after censoring were excluded from the analysis (8 AD patients and 1 HC were excluded). (2) The effect of connectivity density thresholds: We found a consistently decreased clustering coefficient, decreased functional connectivity within the SN, and increased functional connectivity between the SMN and ECN in AD regardless of different threshold values (Table S2 in Supplemental Information). Statistical testing of between-group differences no longer revealed significant effects in characteristic path length, normalized clustering coefficient, normalized characteristic path length, and small-worldness.

## 4. Discussion

Using R-fMRI, dMRI, and graph-based network analysis, we found disrupted functional and structural connectivity patterns in AD. Our main findings are as follows: (1) for the FCN, the global topological organization in AD was significantly and widely disrupted as indicated by abnormal small-world measures (i.e., decreased clustering coefficient, increased characteristic path length, normalized clustering coefficient, normalized characteristic path length, and small-worldness), intramodular and intermodule integration, connections of rich club, and degree values mainly in the temporal gyrus; (2) for the SCN, AD selectively disrupted the characteristic path length, intramodular connections in the DMN, intermodule connections between the ECN and other 4 modules, and degree values in the right middle frontal gyrus, insula, and middle temporal gyrus; and (3) the coupling of functional and structural networks in the hippocampus, insula, frontal gyrus, and middle temporal gyrus was disrupted in AD. These findings advance our understanding of similar and distinct underlying neural mechanisms of AD by different MRI modalities from a network perspective.

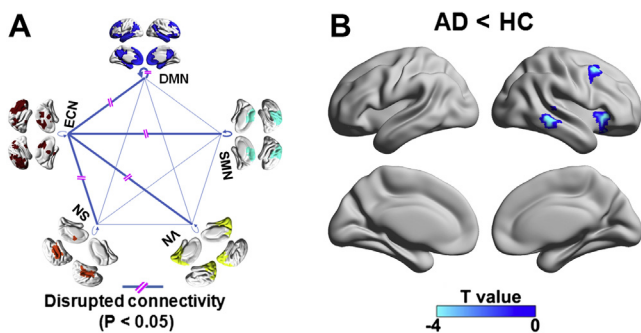


**Fig. 3.** Alterations of modular structure and nodal degree of SCNs in patients with AD relative to HCs. (A) AD-related intramodular and intermodule structural connectivity decrease (*p* < 0.05). The intramodular connectivity was calculated as the sum of the connection within a module, whereas the intermodule connectivity was calculated as the sum of the connection between any pair of 2 modules. The line width represents the t-value of between-group comparison (all AD < HCs). (B) Between-group difference of nodal degree of SCNs (*p* < 0.05, FDR corrected). Abbreviations: SCN, structural connectivity network; DMN, default mode network; SMN, somatosensory-motor network; VN, visual network; SN, salience network; ECN, executive-control network; AD, Alzheimer's disease; HCs, healthy controls.

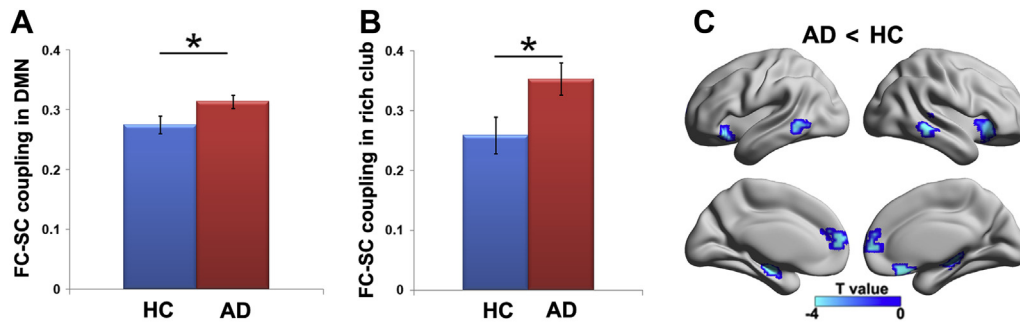


**Fig. 4.** Alterations of functional and structural connectivity coupling in patients with AD relative to HCs. Increased functional and structural connectivity coupling in the DMN (A) and in the rich club (B) in patients with AD compared with HCs. The coupling between FC and SC matrices was examined by computing the correlation between the functional connectivity and structural connectivity. (C) Between-group difference of coupling degree ( $p < 0.05$ , FDR corrected). The coupling degree was calculated as the number of common edges of functional and structural connectivities with the given node. Error bar, standard error of the mean. \* $p < 0.05$ . Abbreviations: AD, Alzheimer's disease; HCs, healthy controls; DMN, default mode network; FC, functional connectivity; SC, structural connectivity.

#### 4.1. Disrupted topology of functional connectivity network

Network studies have revealed a host of attributes that characterize segregation (e.g., clustering coefficient and module structure) and integration (e.g., characteristic path length and rich club) of neural information. Using these measures, we found that the patients with AD had disrupted network segregation (decreased clustering coefficient and increased normalized clustering coefficient) and integration (increased characteristic path length and normalized characteristic path length), which was consistent with previous functional network studies of AD (Zhao et al., 2012). These findings indicated disrupted functional segregation and integration of brain networks in AD. We noted that the results of the clustering coefficient comparison between groups (i.e., decreased clustering coefficient) differ from the results of the normalized clustering coefficient (i.e., increased normalized clustering coefficient). This discrepancy may be due to the statistically significant correlation method that was used here to construct the functional binary network, leading to different numbers of edges in matched random networks for different participants. Another study also found increased characteristic path length accompanied by decreased normalized characteristic path length in AD using magnetoencephalograms (Stam et al., 2009).

In addition to the global level, we also identified the functional connectivity at the subnetwork (i.e., modular structure and rich club organization) and nodal levels. We first found that the functional network of HCs exhibited modular organization with high modularity, which was consistent with previous findings (He et al., 2009b; Power et al., 2011). This modular organization contained 5 main modules: the DMN, ECN, SN, SMN, and VN. The abnormal connections in AD involved both intramodular connectivities within the DMN, ECN, and SN and the intermodule connectivity among the SN, SMN, and VN. These findings are comparable with previous studies of disrupted connectivity within the DMN (Adriaanse et al., 2014; Brier et al., 2012; Buckner, 2004; Dai et al., 2015; Greicius et al., 2004), ECN (Brier et al., 2012; Dai et al., 2015; Li et al., 2012), and SN (Brier et al., 2012; Chen et al., 2013; Dai et al., 2015) in AD. The DMN is involved in a variety of functional processes, including episodic memory and self-related/internally oriented processes (Buckner et al., 2008; Raichle, 2015), and the ECN is related to goal-directed/externally oriented tasks (Dosenbach et al., 2007). The SN mediates the “switching” between activation of the DMN and of the ECN to guide appropriate responses to salient stimuli (Uddin, 2015). These widely disrupted intramodular connections indicated the decline in multiple cognitive functions. Accordingly, the decreased connectivities among SN, SMN, and VN could reflect a reduced ability to detect, orient

attention toward, and react to salient sensory, motor, and visual stimuli in AD. Another intriguing finding was the reduced connection number among the hub regions (i.e., rich club connections), suggesting disrupted global brain functional communication. These results are consistent with previous studies that the GM lesion (Crossley et al., 2014) and functional disconnection (Dai et al., 2015) of AD were mainly concentrated in highly connected brain hubs.

#### 4.2. Disrupted topology of structural connectivity network

Our results revealed that the structural network of the AD group showed significantly increased characteristic path length compared with HCs. These results are consistent with previous structural brain network studies in AD (He et al., 2008; Lo et al., 2010). Characteristic path length reflects interregional effective information integrity in the brain network, which underlies cognitive processing (Sporns and Zwi, 2004). Thus, the AD-related increases in the characteristic path length between regions may be related to the degeneration of fiber bundles used for information transmission.

We also found that the within-module structural connection number decreased in the DMN of AD, which was consistent with the previous study (Hahn et al., 2013). In addition, the structural connection number between ECN and DMN and that between ECN and SN were found to decrease as well. The triple network model of the DMN, SN, and ECN has been used to investigate cognitive and affective dysfunction in neurological diseases (Menon, 2011). The decreased connections between the ECN and DMN could lead to weak competitive processes between externally goal-directed attention and internally oriented processes in AD, which was supported by the loss of anticorrelation of functional connectivity between the DMN and ECN in AD (Agosta et al., 2012; Brier et al., 2012). The decreased connections between the ECN and SN could reflect aberrant control signals to the ECN that facilitate access to externally goal-directed attention. The decreased connections between the ECN and VN and that between ECN and SMN could reflect reduced executive ability to external stimulus, including sensorimotor stimuli and visual stimuli. Notably, AD had relatively preserved connectivity within the rich club in SCNs, which was consistent with a previous study (Daianu et al., 2015). However, these results do not mean that the hub nodes are not affected at the regional level. The decreased nodal degree was found in the right insula in the present study, which is a hub region of structural networks (Collin et al., 2014).

Examination of the FCN and SCN consistently showed increased characteristic path length and decreased intramodular connections in the DMN of AD (Table 2), suggesting a disrupted integration and

segregation topological organization in AD. In contrast, more widely disrupted topological measures of FCNs in AD compared with SCNs were found (Table 2), implying that the FCNs may be more sensitive to detect the abnormalities in AD than the SCNs, which was accordant with the hypothetical model of biomarkers of AD (Sperling et al., 2011). This model suggests a typical AD deterioration process with abnormal  $\beta$ -amyloid (the core neuropathology of AD) accumulation occurring first, followed sequentially by disturbance of the function of neurons and synapses, disruption of the brain structure, and, finally, the appearance of clinical symptoms.

#### 4.3. Decoupling between structural and functional connectivity

Although the network measures of both functional and structural networks were significantly decreased in AD, increased couplings between functional and structural networks (i.e., DMN module and the rich club structure) were found in patients with AD. These increased couplings may suggest that AD leads to a strengthened relationship between functional connectivity and the underlying anatomical connectivity, which may imply more-stringent and less-dynamic brain function in AD. On the other hand, these results indicated that structural connectivity can better predict functional connectivity in patients with AD than HCs. A stronger correlation between structural and functional networks was also observed in patients with schizophrenia (van den Heuvel et al., 2013). Intriguingly, these enhanced couplings between functional and structural connectivities were found in the DMN module and rich club connections. These 2 essential components of the brain play a core role in optimizing global brain communication and are associated with higher cognitive functions. The strengthened FC-SC couplings in the 2 elements of AD may lead to consistent changes in FC and SC in the DMN or rich club. Indeed, we found the commonly disrupted structural and functional connectivity in the DMN in AD. However, we did not find similar results in the rich club, as decreased functional connectivity along with relatively preserved structural connectivity within the rich club was found. This could be because abnormal functional connectivity emerges before disruptions in structural connectivity become apparent (Sperling et al., 2011). This hypothesis was supported by our findings of the broad abnormal network measures of the functional network compared with the structural network in AD.

A significantly decreased coupling degree was found in the frontal lobe (e.g., the medial prefrontal gyrus, inferior frontal gyrus, and rectus), temporal lobe (e.g., the middle temporal gyrus and hippocampus), and insula. These regions are involved in high-level cognitive functions such as episodic memory, attention, motivation, self-awareness, and audio-visual integration, which are the main deficiencies in patients with AD. Previous studies have demonstrated AD-related abnormalities in the frontal lobe (Dai et al., 2015; Lo et al., 2010), temporal lobe (Dore et al., 2013; Supekar et al., 2008; Zhou et al., 2008), and insula (Blanc et al., 2014; Dai et al., 2015).

#### 4.4. Limitations and further considerations

Several issues need to be considered further. First, diffusion tensor imaging and deterministic tractography methods were used here to construct the structural network. However, the tracking procedure of this method always terminates when it arrives at a voxel with fiber crossing or spreading, which leads to the loss of tracking the existing fibers. Further studies could use more advanced diffusion acquisitions and diffusion models, such as high angular resolution imaging (Tuch et al., 2002) and probabilistic tractography (Behrens et al., 2007), to reconstruct more accurate anatomical connectivity.

Second, functional connectivity was used here to construct the functional network, which is a result of the correlation between the time series of each pair of ROIs. The advent of informational connectivity analyses could explore the interactions between ROIs using the information encoded in the multivoxel pattern (Anzellotti and Coutanche, 2018; Coutanche and Thompson-Schill, 2013), which is ignored by the correlation method. Further studies could use informational connectivity to reconstruct the functional networks to capture communication of information throughout the whole brain.

Third, a number of neuroimaging studies have demonstrated that head motion can introduce systematic artifacts and has a confounding effect on functional connectivity (Power et al., 2012; Satterthwaite et al., 2013; Van Dijk et al., 2012; Yan et al., 2013). In the main analyses, we used CompCor and 24 head motion parameters regression in data preprocessing to correct this motion artifact. To validate our results, the mean FD regression and scrubbing methods were used as alternative head motion correction strategies. We found that our main results were not affected while using the 2 different strategies, suggesting the reliability of our findings. Interestingly, we also noticed that there were more between-group differences in the results of FCNs when using the scrubbing and regressing out the FD strategies. These results suggest that different motion correction strategies may produce consistent and specific findings. Future studies need to validate which head motion correction strategy could be appropriate for AD research. Notably, the effects of residual motion might still exist as the full impact of head motion on functional connectivity is not yet clear and the methods to offset influences of the head motion are still being developed and validated (for review, see Power et al., 2015). Moreover, we used a related lenient FD threshold (i.e., 0.5 mm) for the scrubbing method because the elderly participants had poor control ability. Even so, to ensure the reliability of the results, 9 participants were excluded in the subsequent analysis because they had less than 5 minutes of R-fMRI data after censoring. Therefore, our results should be further validated when better head motion correction methods have been developed.

Fourth, for brain network studies, the selection of thresholding procedures is still a controversial topic (van den Heuvel et al., 2017). There are currently 2 main types of thresholding procedures: the fixed-density threshold and the fixed-correlation threshold (the method used in this article). The fixed-density threshold may introduce nonsignificant correlations (for matrices with low average connectivity), which may increase random noisy connections and make the network more like randomly connected networks (van den Heuvel et al., 2017). The fixed-correlation threshold may lead to different numbers of edges in the resulting networks, which could confound between-group topological comparisons (Van Wijk et al., 2010). Different thresholding methods may lead to different topological organizations and further lead to different results when making between-group comparisons. Here, we consistently found decreased clustering coefficient and decreased functional connectivity within the SN in AD regardless of different threshold values (Table S3 in Supplemental Information), which were consistent with our results with the fixed-correlation threshold method. However, other significant results of our main findings were no longer revealed as significant between-group differences with the fixed-density thresholding method. The discrepancies between the results obtained by the 2 different thresholding methods indicated that our main findings are dependent on the choice of the thresholding methods and are influenced by different numbers of connections. Therefore, the different conceptual features of 2 thresholding strategies should be kept in mind in future network analysis of contrastive research.

Fifth, the current findings showed that the functional connection numbers were significantly reduced in AD for rich club connections when  $k$  varied from 11 to 13. This finding indicated that the effect of the abnormal rich club connections of the functional network in AD was robustly related to the choice of  $k$  values. Meanwhile, significantly increased FC-SC correlations were found in the rich club connections of the AD group compared with the HC group when  $k$  equaled 17. The result suggested that the effect of the abnormal FC-SC correlation in rich club connections in AD was sensitive to the choice of  $k$  values and that this disrupted coupling in AD was only found in the connections among a small fraction of high-degree nodes ( $\sim 5\%$ ). Therefore, our results of rich club depended on the choice of the  $k$  values.

Sixth, the correlation results between network metrics and cognitive performance were not significant after FDR correction. There are 2 possible reasons: one was that the small sample size leads to the underpowered; and the other one was that our study, which was exploratory in nature, resulting in many statistical comparisons. In the future, confirmatory studies in a larger independent data set with a priori hypotheses restricting the number of statistical tests are needed.

Seventh, the increased FCN-SCN coupling was found in this study. AD-related longitudinal studies are vital in the future to explore whether such coupling increases with the disease progression. If so, parameters that describe the FCN-SCN coupling should be added to the computational model that simulates the spread of AD for enhancement of the accuracy of these models.

Eighth, the core neuropathologies of AD are the accumulation of  $\beta$ -amyloid and hyperphosphorylated *tau*, which can be detected by positron emission tomography. The relationships between these pathological changes and network measure abnormalities through MRI data require investigation of the pathological factors contributing to the abnormal network measures of FCN and SCN, including identifying the overlapping regions from the various techniques and causal relationships. These findings can deepen our understanding of the pathophysiological mechanisms of FCN and SCN disruptions. In addition, researchers in this area should be constantly vigilant that abnormalities in these network measures assessed by R-fMRI could be caused by the altered vascular physiology that is unrelated to the neural activity changes (D'Esposito et al., 2003) because the R-fMRI indirectly measures neuronal activity through the blood-oxygen-level-dependent signal, which depends on neurovascular coupling.

## 5. Conclusions

Using the graph-theory network analysis, the present study demonstrated that relative to the HC group, patients with AD exhibited reduced network integrity (i.e., increased characteristic path length) and network segregation (i.e., reduced intramodular connections on the DMN) in both the FCN and SCN. Moreover, the FCN of AD additionally showed reduced clustering coefficient and rich club connections. Finally, we found the increased coupling between the FCN and SCN in the connections of DMN and the rich club. Taken together, these findings highlight disrupted topological organization of the FCN and SCN in the same cohort of AD and provide empirical evidence that the combination of graph-theory network analysis and multimodal MRI technology is a promising research framework to investigate the pathophysiological mechanisms of AD.

## Disclosure statement

The authors have no actual or potential conflicts of interest.

## Acknowledgements

This work was supported by the Ministry of Science and Technology (2017YFC1311100), National Natural Science Foundation of China (No. 81620108016, 81601559, and 81171018), Guangdong Provincial Natural Science Foundation of China (No. 2016A030310233), Changjiang Scholar Professorship Award (T2015027), Beijing Natural Science Foundation (No. Z161100004916027 and Z151100003915082), and Fundamental Research Funds for the Central Universities (No. 2017XTX04).

## Appendix A. Supplementary data

Supplementary data to this article can be found online at <https://doi.org/10.1016/j.neurobiolaging.2018.11.005>.

## References

- Adriaanse, S.M., Binnewijzend, M.A., Ossenkoppele, R., Tijms, B.M., van der Flier, W.M., Koene, T., Smits, L.L., Wink, A.M., Scheltens, P., van Berckel, B.N., Barkhof, F., 2014. Widespread disruption of functional brain organization in early-onset Alzheimer's disease. *PLoS One* 9, e102995.
- Agosta, F., Pievani, M., Geroldi, C., Copetti, M., Frisoni, G.B., Filippi, M., 2012. Resting state fMRI in Alzheimer's disease: beyond the default mode network. *Neurobiol. Aging* 33, 1564–1578.
- Alexander-Bloch, A., Raznahan, A., Bullmore, E., Giedd, J., 2013. The convergence of maturational change and structural covariance in human cortical networks. *J. Neurosci.* 33, 2889–2899.
- Anzellotti, S., Coutanche, M.N., 2018. Beyond functional connectivity: investigating networks of multivariate representations. *Trends Cogn. Sci.* 22, 258–269.
- Ashburner, J., Friston, K.J., 2005. Unified segmentation. *Neuroimage* 26, 839–851.
- Behrens, T.E., Berg, H.J., Jbabdi, S., Rushworth, M.F., Woolrich, M.W., 2007. Probabilistic diffusion tractography with multiple fibre orientations: what can we gain? *Neuroimage* 34, 144–155.
- Behzadi, Y., Restom, K., Liu, J., Liu, T.T., 2007. A component based noise correction method (CompCor) for BOLD and perfusion based fMRI. *Neuroimage* 37, 90–101.
- Biswal, B., Yetkin, F.Z., Haughton, V.M., Hyde, J.S., 1995. Functional connectivity in the motor cortex of resting human brain using echo-planar MRI. *Magn. Reson. Med.* 34, 537–541.
- Blanc, F., Noblet, V., Philippi, N., Cretin, B., Foucher, J., Armspach, J.-P., Rousseau, F., Initiative, A.S.D.N., 2014. Right anterior insula: core region of hallucinations in cognitive neurodegenerative diseases. *PLoS One* 9, e114774.
- Brier, M.R., Thomas, J.B., Snyder, A.Z., Benzinger, T.L., Zhang, D., Raichle, M.E., Holtzman, D.M., Morris, J.C., Ances, B.M., 2012. Loss of intranetwork and internetwork resting state functional connections with Alzheimer's disease progression. *J. Neurosci.* 32, 8890–8899.
- Buckner, R.L., 2004. Memory and executive function in aging and AD: multiple factors that cause decline and reserve factors that compensate. *Neuron* 44, 195–208.
- Buckner, R.L., Andrews-Hanna, J.R., Schacter, D.L., 2008. The brain's default network: anatomy, function, and relevance to disease. *Ann. N. Y. Acad. Sci.* 1124, 1–38.
- Bullmore, E., Sporns, O., 2009. Complex brain networks: graph theoretical analysis of structural and functional systems. *Nat. Rev. Neurosci.* 10, 186–198.
- Chen, G., Zhang, H.Y., Xie, C., Chen, G., Zhang, Z.J., Teng, G.J., Li, S.J., 2013. Modular reorganization of brain resting state networks and its independent validation in Alzheimer's disease patients. *Front. Hum. Neurosci.* 7, 456.
- Chen, X., Lu, B., Yan, C.G., 2018. Reproducibility of R-fMRI metrics on the impact of different strategies for multiple comparison correction and sample sizes. *Hum. Brain Mapp.* 39, 300–318.
- Cohen, J.R., D'Esposito, M., 2016. The segregation and integration of distinct brain networks and their relationship to cognition. *J. Neurosci.* 36, 12083–12094.
- Colizza, V., Flammini, A., Serrano, M.A., Vespignani, A., 2006. Detecting rich-club ordering in complex networks. *Nat. Phys.* 2, 110.
- Collignon, A., Maes, F., Delaere, D., Vandermeulen, D., Suetens, P., Marchal, G., 1995. Automated multi-modality image registration based on information theory. *Inf. Process. Med. Imaging* 3, 263–274.
- Collin, G., Sporns, O., Mandl, R.C., van den Heuvel, M.P., 2014. Structural and functional aspects relating to cost and benefit of rich club organization in the human cerebral cortex. *Cereb. Cortex* 24, 2258–2267.
- Coutanche, M.N., Thompson-Schill, S.L., 2013. Informational connectivity: identifying synchronized discriminability of multi-voxel patterns across the brain. *Front. Hum. Neurosci.* 7, 15.
- Crossley, N.A., Mechelli, A., Scott, J., Carletti, F., Fox, P.T., McGuire, P., Bullmore, E.T., 2014. The hubs of the human connectome are generally implicated in the anatomy of brain disorders. *Brain* 137, 2382–2395.
- Crossley, N.A., Mechelli, A., Vertes, P.E., Winton-Brown, T.T., Patel, A.X., Ginestet, C.E., McGuire, P., Bullmore, E.T., 2013. Cognitive relevance of the community

- structure of the human brain functional coactivation network. *Proc. Natl. Acad. Sci. U. S. A.* 110, 11583–11588.
- D'Esposito, M., Deouell, L.Y., Gazzaley, A., 2003. Alterations in the BOLD fMRI signal with ageing and disease: a challenge for neuroimaging. *Nat. Rev. Neurosci.* 4, 863.
- Dai, Z., He, Y., 2014. Disrupted structural and functional brain connectomes in mild cognitive impairment and Alzheimer's disease. *Neurosci. Bull.* 30, 217–232.
- Dai, Z., Yan, C., Li, K., Wang, Z., Wang, J., Cao, M., Lin, Q., Shu, N., Xia, M., Bi, Y., He, Y., 2015. Identifying and mapping connectivity patterns of brain network hubs in Alzheimer's disease. *Cereb. Cortex* 25, 3723–3742.
- Daianu, M., Jahanshad, N., Nir, T.M., Jack Jr., C.R., Weiner, M.W., Bernstein, M.A., Thompson, P.M., 2015. Rich club analysis in the Alzheimer's disease connectome reveals a relatively undisturbed structural core network. *Hum. Brain Mapp.* 36, 3087–3103.
- Daianu, M., Jahanshad, N., Nir, T.M., Toga, A., Jack, C.R., Weiner, M.W., Thompson, P., 2013. Breakdown of brain connectivity between normal aging and Alzheimer's disease: a structural k-core network analysis. *Brain Connect.* 3, 407–422.
- Delbeuck, X., Collette, F., Van der Linden, M., 2007. Is Alzheimer's disease a disconnection syndrome? *Neuropsychologia* 45, 3315–3323.
- Delbeuck, X., Van der Linden, M., Collette, F., 2003. Alzheimer's disease as a disconnection syndrome? *Neuropsychol. Rev.* 13, 79–92.
- Dick, M., Teng, E., Kempler, D., Davis, D., Taussig, I., 2002. The cross-cultural neuropsychological test battery (CCNB): effects of age, education, ethnicity, and cognitive status on performance. *Minority and Cross-cultural Aspects of Neuropsychological Assessment*. Lisse, The Netherlands, Swets & Zeitlinger.
- Doré, V., Villemagne, V.L., Bourgeat, P., Fripp, J., Acosta, O., Chetelat, G., Zhou, L., Martins, R., Ellis, K.A., Masters, C.L., 2013. Cross-sectional and longitudinal analysis of the relationship between A $\beta$  deposition, cortical thickness, and memory in cognitively unimpaired individuals and in Alzheimer disease. *JAMA Neurol.* 70, 903–911.
- Dosenbach, N.U., Fair, D.A., Miezin, F.M., Cohen, A.L., Wenger, K.K., Dosenbach, R.A., Fox, M.D., Snyder, A.Z., Vincent, J.L., Raichle, M.E., Schlaggar, B.L., Petersen, S.E., 2007. Distinct brain networks for adaptive and stable task control in humans. *Proc. Natl. Acad. Sci. U. S. A.* 104, 11073–11078.
- Fox, M.D., Zhang, D., Snyder, A.Z., Raichle, M.E., 2009. The global signal and observed anticorrelated resting state brain networks. *J. Neurophysiol.* 101, 3270–3283.
- Friston, K.J., Williams, S., Howard, R., Frackowiak, R.S., Turner, R., 1996. Movement-related effects in fMRI time-series. *Magn. Reson. Med.* 35, 346–355.
- Geib, B.R., Stanley, M.L., Dennis, N.A., Woldorff, M.G., Cabeza, R., 2017. From hippocampus to whole-brain: the role of integrative processing in episodic memory retrieval. *Hum. Brain Mapp.* 38, 2242–2259.
- Gong, G., He, Y., Concha, L., Lebel, C., Gross, D.W., Evans, A.C., Beaulieu, C., 2009. Mapping anatomical connectivity patterns of human cerebral cortex using in vivo diffusion tensor imaging tractography. *Cereb. Cortex* 19, 524–536.
- Greicius, M.D., Srivastava, G., Reiss, A.L., Menon, V., 2004. Default-mode network activity distinguishes Alzheimer's disease from healthy aging: evidence from functional MRI. *Proc. Natl. Acad. Sci. U. S. A.* 101, 4637–4642.
- Greicius, M.D., Supekar, K., Menon, V., Dougherty, R.F., 2009. Resting-state functional connectivity reflects structural connectivity in the default mode network. *Cereb. Cortex* 19, 72–78.
- Hagmann, P., Sporns, O., Madan, N., Cammoun, L., Pienaar, R., Wedeen, V.J., Meuli, R., Thiran, J.P., Grant, P.E., 2010. White matter maturation reshapes structural connectivity in the late developing human brain. *Proc. Natl. Acad. Sci. U. S. A.* 107, 19067–19072.
- Hahn, K., Myers, N., Prigarin, S., Rodenacker, K., Kurz, A., Forstl, H., Zimmer, C., Wohlschläger, A.M., Sorg, C., 2013. Selectively and progressively disrupted structural connectivity of functional brain networks in Alzheimer's disease - revealed by a novel framework to analyze edge distributions of networks detecting disruptions with strong statistical evidence. *Neuroimage* 81, 96–109.
- He, Y., Chen, Z., Evans, A., 2008. Structural insights into aberrant topological patterns of large-scale cortical networks in Alzheimer's disease. *J. Neurosci.* 28, 4756–4766.
- He, Y., Chen, Z., Gong, G., Evans, A., 2009a. Neuronal networks in Alzheimer's disease. *Neuroscientist* 15, 333–350.
- He, Y., Evans, A., 2010. Graph theoretical modeling of brain connectivity. *Curr. Opin. Neurol.* 23, 341–350.
- He, Y., Wang, J., Wang, L., Chen, Z.J., Yan, C., Yang, H., Tang, H., Zhu, C., Gong, Q., Zang, Y., Evans, A.C., 2009b. Uncovering intrinsic modular organization of spontaneous brain activity in humans. *PLoS One* 4, e5226.
- Hermundstad, A.M., Bassett, D.S., Brown, K.S., Aminoff, E.M., Clewett, D., Freeman, S., Frithsen, A., Johnson, A., Tipper, C.M., Miller, M.B., Grafton, S.T., Carlson, J.M., 2013. Structural foundations of resting-state and task-based functional connectivity in the human brain. *Proc. Natl. Acad. Sci. U. S. A.* 110, 6169–6174.
- Honey, C.J., Sporns, O., Cammoun, L., Gigandet, X., Thiran, J.P., Meuli, R., Hagmann, P., 2009. Predicting human resting-state functional connectivity from structural connectivity. *Proc. Natl. Acad. Sci. U. S. A.* 106, 2035–2040.
- Honey, C.J., Thivierge, J.P., Sporns, O., 2010. Can structure predict function in the human brain? *Neuroimage* 52, 766–776.
- Jenkinson, M., Bannister, P., Brady, M., Smith, S., 2002. Improved optimization for the robust and accurate linear registration and motion correction of brain images. *Neuroimage* 17, 825–841.
- Kempler, D., Teng, E.L., Taussig, M., Dick, M.B., 2010. The common objects memory test (COMT): a simple test with cross-cultural applicability. *J. Int. Neuropsychol.* 16, 537–545.
- Lancichinetti, A., Fortunato, S., Kertész, J., 2008. Detecting the overlapping and hierarchical community structure of complex networks. *N. J. Phys.* 11, 19–44.
- Li, R., Wu, X., Fleisher, A.S., Reiman, E.M., Chen, K., Yao, L., 2012. Attention-related networks in Alzheimer's disease: a resting functional MRI study. *Hum. Brain Mapp.* 33, 1076–1088.
- Liang, X., Zou, Q., He, Y., Yang, Y., 2013. Coupling of functional connectivity and regional cerebral blood flow reveals a physiological basis for network hubs of the human brain. *Proc. Natl. Acad. Sci. U. S. A.* 110, 1929–1934.
- Liang, X., Zou, Q., He, Y., Yang, Y., 2015. Topologically reorganized connectivity architecture of default-mode, executive-control, and salience networks across working memory task loads. *Cereb. Cortex* 26, 1501–1511.
- Liao, X., Vasilakos, A.V., He, Y., 2017. Small-world human brain networks: perspectives and challenges. *Neurosci. Biobehav. Rev.* 77, 286–300.
- Liao, X., Xia, M., Xu, T., Dai, Z., Cao, X., Niu, H., Zuo, X., Zang, Y., He, Y., 2013. Functional brain hubs and their test-retest reliability: a multiband resting-state functional MRI study. *Neuroimage* 83, 969–982.
- Lo, C.Y., Wang, P.N., Chou, K.H., Wang, J., He, Y., Lin, C.P., 2010. Diffusion tensor tractography reveals abnormal topological organization in structural cortical networks in Alzheimer's disease. *J. Neurosci.* 30, 16876–16885.
- Lowe, M.J., Mock, B.J., Sorenson, J.A., 1998. Functional connectivity in single and multi-echo planar imaging using resting-state fluctuations. *Neuroimage* 7, 119–132.
- McKhann, G., Drachman, D., Folstein, M., Katzman, R., Price, D., Stadlan, E.M., 1984. Clinical diagnosis of Alzheimer's disease: report of the NINCDS-ADRDA work group under the auspices of Department of Health and Human Services task Force on Alzheimer's disease. *Neurology* 34, 939–944.
- Menon, V., 2011. Large-scale brain networks and psychopathology: a unifying triple network model. *Trends Cogn. Sci.* 15, 483–506.
- Mori, S., Crain, B.J., Chacko, V.P., van Zijl, P.C., 1999. Three-dimensional tracking of axonal projections in the brain by magnetic resonance imaging. *Ann. Neurol.* 45, 265–269.
- Morris, J.C., 1993. The Clinical Dementia Rating (CDR): current version and scoring rules. *Neurology* 43, 2412–2414.
- Murphy, K., Birn, R.M., Handwerker, D.A., Jones, T.B., Bandettini, P.A., 2009. The impact of global signal regression on resting state correlations: are anti-correlated networks introduced? *Neuroimage* 44, 893–905.
- Muschelli, J., Nebel, M.B., Caffo, B.S., Barber, A.D., Pekar, J.J., Mostofsky, S.H., 2014. Reduction of motion-related artifacts in resting state fMRI using aCompCor. *Neuroimage* 96, 22–35.
- Newman, M.E., 2006. Modularity and community structure in networks. *Proc. Natl. Acad. Sci. U. S. A.* 103, 8577–8582.
- Park, C.H., Kim, S.Y., Kim, Y.-H., Kim, K., 2008. Comparison of the small-world topology between anatomical and functional connectivity in the human brain. *Phys. Stat. Mech. Appl.* 387, 5958–5962.
- Park, H.J., Friston, K., 2013. Structural and functional brain networks: from connections to cognition. *Science* 342, 1238411.
- Power, J.D., Barnes, K.A., Snyder, A.Z., Schlaggar, B.L., Petersen, S.E., 2012. Spurious but systematic correlations in functional connectivity MRI networks arise from subject motion. *Neuroimage* 59, 2142–2154.
- Power, J.D., Cohen, A.L., Nelson, S.M., Wig, G.S., Barnes, K.A., Church, J.A., Vogel, A.C., Laumann, T.O., Miezin, F.M., Schlaggar, B.L., Petersen, S.E., 2011. Functional network organization of the human brain. *Neuron* 72, 665–678.
- Power, J.D., Schlaggar, B.L., Petersen, S.E., 2015. Recent progress and outstanding issues in motion correction in resting state fMRI. *Neuroimage* 105, 536–551.
- Raichle, M.E., 2015. The brain's default mode network. *Annu. Rev. Neurosci.* 38, 433–447.
- Rubinov, M., Sporns, O., 2010. Complex network measures of brain connectivity: uses and interpretations. *Neuroimage* 52, 1059–1069.
- Sanz-Arigita, E.J., Schoonheim, M.M., Damoiseaux, J.S., Rombouts, S.A., Maris, E., Barkhof, F., Scheltens, P., Stam, C.J., 2010. Loss of 'small-world' networks in Alzheimer's disease: graph analysis of FMRI resting-state functional connectivity. *PLoS One* 5, e13788.
- Satterthwaite, T.D., Elliott, M.A., Gerraty, R.T., Ruparel, K., Loughhead, J., Calkins, M.E., Eickhoff, S.B., Hakonarson, H., Gur, R.C., Gur, R.E., Wolf, D.H., 2013. An improved framework for confound regression and filtering for control of motion artifact in the preprocessing of resting-state functional connectivity data. *Neuroimage* 64, 240–256.
- Shu, N., Liu, Y., Li, K., Duan, Y., Wang, J., Yu, C., Dong, H., Ye, J., He, Y., 2011. Diffusion tensor tractography reveals disrupted topological efficiency in white matter structural networks in multiple sclerosis. *Cereb. Cortex* 21, 2565–2577.
- Skudlarski, P., Jagannathan, K., Calhoun, V.D., Hampson, M., Skudlarska, B.A., Pearlson, G., 2008. Measuring brain connectivity: diffusion tensor imaging validates resting state temporal correlations. *Neuroimage* 43, 554–561.
- Sperling, R.A., Aisen, P.S., Beckett, L.A., Bennett, D.A., Craft, S., Fagan, A.M., Iwatsubo, T., Jack Jr., C.R., Kaye, J., Montine, T.J., Park, D.C., Reiman, E.M., Rowe, C.C., Siemers, E., Stern, Y., Yaffe, K., Carrillo, M.C., Thies, B., Morrison-Bogorad, M., Wagster, M.V., Phelps, C.H., 2011. Toward defining the preclinical stages of Alzheimer's disease: recommendations from the National Institute on Aging-Alzheimer's Association workgroups on diagnostic guidelines for Alzheimer's disease. *Alzheimer's Demen.* 7, 280–292.
- Sporns, O., Tononi, G., Kotter, R., 2005. The human connectome: a structural description of the human brain. *PLoS Comput. Biol.* 1, e42.
- Sporns, O., Zwi, J.D., 2004. The small world of the cerebral cortex. *Neuroinformatics* 2, 145–162.

- Stam, C.J., de Haan, W., Daffertshofer, A., Jones, B.F., Manshanden, I., van Cappellen van Walsum, A.M., Montez, T., Verbunt, J.P., de Munck, J.C., van Dijk, B.W., Berendse, H.W., Scheltens, P., 2009. Graph theoretical analysis of magnetoencephalographic functional connectivity in Alzheimer's disease. *Brain* 132, 213–224.
- Supekar, K., Menon, V., Rubin, D., Musen, M., Greicius, M.D., 2008. Network analysis of intrinsic functional brain connectivity in Alzheimer's disease. *PLoS Comput. Biol.* 4, e1000100.
- Teng, E.L., Hasegawa, K., Homma, A., Imai, Y., Larson, E., Graves, A., Sugimoto, K., Yamaguchi, T., Sasaki, H., Chiu, D., White, L.R., 1994. The Cognitive Abilities Screening Instrument (CASI): a practical test for cross-cultural epidemiological studies of dementia. *Int. Psychogeriatr.* 6, 45–58.
- Tijms, B.M., Wink, A.M., de Haan, W., van der Flier, W.M., Stam, C.J., Scheltens, P., Barkhof, F., 2013. Alzheimer's disease: connecting findings from graph theoretical studies of brain networks. *Neurobiol. Aging* 34, 2023–2036.
- Tomasi, D., Wang, G.J., Volkow, N.D., 2013. Energetic cost of brain functional connectivity. *Proc. Natl. Acad. Sci. U. S. A.* 110, 13642–13647.
- Tuch, D.S., Reese, T.G., Wiegell, M.R., Makris, N., Belliveau, J.W., Wedeen, V.J., 2002. High angular resolution diffusion imaging reveals intravoxel white matter fiber heterogeneity. *Magn. Reson. Med.* 48, 577–582.
- Tzourio-Mazoyer, N., Landeau, B., Papathanassiou, D., Crivello, F., Etard, O., Delcroix, N., Mazoyer, B., Joliot, M., 2002. Automated anatomical labeling of activations in SPM using a macroscopic anatomical parcellation of the MNI MRI single-subject brain. *Neuroimage* 15, 273–289.
- Uddin, L.Q., 2015. Salience processing and insular cortical function and dysfunction. *Nat. Rev. Neurosci.* 16, 55–61.
- Vaishnavi, S.N., Vlassenko, A.G., Rundle, M.M., Snyder, A.Z., Mintun, M.A., Raichle, M.E., 2010. Regional aerobic glycolysis in the human brain. *Proc. Natl. Acad. Sci. U. S. A.* 107, 17757–17762.
- van den Heuvel, M.P., de Lange, S.C., Zalesky, A., Seguin, C., Yeo, B.T., Schmidt, R., 2017. Proportional thresholding in resting-state fMRI functional connectivity networks and consequences for patient-control connectome studies: issues and recommendations. *Neuroimage* 152, 437–449.
- van den Heuvel, M.P., Mandl, R.C., Kahn, R.S., Hulshoff Pol, H.E., 2009. Functionally linked resting-state networks reflect the underlying structural connectivity architecture of the human brain. *Hum. Brain Mapp.* 30, 3127–3141.
- van den Heuvel, M.P., Sporns, O., 2011. Rich-club organization of the human connectome. *J. Neurosci.* 31, 15775–15786.
- van den Heuvel, M.P., Sporns, O., Collin, G., Scheewe, T., Mandl, R.C., Cahn, W., Goni, J., Hulshoff Pol, H.E., Kahn, R.S., 2013. Abnormal rich club organization and functional brain dynamics in schizophrenia. *JAMA Psychiatr.* 70, 783–792.
- Van Dijk, K.R., Sabuncu, M.R., Buckner, R.L., 2012. The influence of head motion on intrinsic functional connectivity MRI. *Neuroimage* 59, 431–438.
- Van Wijk, B.C., Stam, C.J., Daffertshofer, A., 2010. Comparing brain networks of different size and connectivity density using graph theory. *PLoS one* 5, e13701.
- Wang, J., Wang, X., He, Y., Yu, X., Wang, H., He, Y., 2015a. Apolipoprotein E epsilon4 modulates functional brain connectome in Alzheimer's disease. *Hum. Brain Mapp.* 36, 1828–1846.
- Wang, J., Zuo, X., Gohel, S., Milham, M.P., Biswal, B.B., He, Y., 2011. Graph theoretical analysis of functional brain networks: test-retest evaluation on short- and long-term resting-state functional MRI data. *PLoS One* 6, e21976.
- Wang, X., Wang, J., He, Y., Li, H., Yuan, H., Evans, A., Yu, X., He, Y., Wang, H., 2015b. Apolipoprotein E epsilon4 modulates cognitive profiles, hippocampal volume, and resting-state functional connectivity in Alzheimer's disease. *J. Alzheimers Dis.* 45, 781–795.
- Wang, Z., Dai, Z., Gong, G., Zhou, C., He, Y., 2015c. Understanding structural-functional relationships in the human brain: a large-scale network perspective. *Neuroscientist* 21, 290–305.
- World Health Organization, 1999. International Classification of Diseases, 10th Revision (ICD-10). World Health Organization, Geneva.
- Xia, M., Wang, J., He, Y., 2013. BrainNet Viewer: a network visualization tool for human brain connectomics. *PLoS One* 8, e68910.
- Yan, C., Cheung, B., Kelly, C., Colcombe, S., Craddock, R.C., Di Martino, A., Li, Q., Zuo, X., Castellanos, F.X., Milham, M.P., 2013. A comprehensive assessment of regional variation in the impact of head micromovements on functional connectomics. *Neuroimage* 76, 183–201.
- Yan, C., Zang, Y., 2010. DPARSF: a MATLAB Toolbox for "Pipeline" data analysis of resting-state fMRI. *Front. Syst. Neurosci.* 4, 13.
- Yeo, B.T., Krienen, F.M., Sepulcre, J., Sabuncu, M.R., Lashkari, D., Hollinshead, M., Roffman, J.L., Smoller, J.W., Zollei, L., Polimeni, J.R., Fischl, B., Liu, H., Buckner, R.L., 2011. The organization of the human cerebral cortex estimated by intrinsic functional connectivity. *J. Neurophysiol.* 106, 1125–1165.
- Zalesky, A., Fornito, A., Harding, I.H., Cocchi, L., Yücel, M., Pantelis, C., Bullmore, E.T., 2010. Whole-brain anatomical networks: does the choice of nodes matter? *Neuroimage* 50, 970–983.
- Zhang, Z., Liao, W., Chen, H., Mantini, D., Ding, J.R., Xu, Q., Wang, Z., Yuan, C., Chen, G., Jiao, Q., Lu, G., 2011. Altered functional-structural coupling of large-scale brain networks in idiopathic generalized epilepsy. *Brain* 134, 2912–2928.
- Zhao, X., Liu, Y., Wang, X., Liu, B., Xi, Q., Guo, Q., Jiang, H., Jiang, T., Wang, P., 2012. Disrupted small-world brain networks in moderate Alzheimer's disease: a resting-state fMRI study. *PLoS One* 7, e33540.
- Zhou, Y., Dougherty, J.H., Hubner, K.F., Bai, B., Cannon, R.L., Hutson, R.K., 2008. Abnormal connectivity in the posterior cingulate and hippocampus in early Alzheimer's disease and mild cognitive impairment. *Alzheimer's Dement. J. Alzheimer's Assoc.* 4, 265–270.